https://dx.doi.org/10.21577/0103-5053.20220064

J. Braz. Chem. Soc., Vol. 33, No. 11, 1332-1341, 2022

Article

Effect of Multi-Pass Rolling on the Performance of AZ31 Magnesium Alloy Anode in Mg-Air Battery

Jinchao Zou,[a,b] *Junpeng Wang,*[a,b] *Zhiquan Huang**[,a,b] *and Tao Zhang*[a,b]

[a]*Heavy Machinery Engineering Research Center of the Ministry of Education, Taiyuan University of Science and Technology, 030024 Taiyuan, China*

[b]*School of Mechanical Engineering, Taiyuan University of Science and Technology, 030024 Taiyuan, China*

In this work, the influence of rolling passes on microstructure, corrosion behavior, electrochemical performance, and battery performance of AZ31 magnesium alloy was studied. The experimental results show that the grain size decreases first and then increases with rolling passes. Among them, the grain size of three passes rolled sample is the smallest, while the grain size of the four passes rolled sample is obviously refined and evenly distributed, accompanied by a small number of twins. Therefore, it exhibits more muscular discharge activity. In addition, the corrosion products of the four passes rolled samples are distributed loosely and evenly on the surface during immersion, which is easy to fall off, thus reducing the polarization. The surface of the discharged four passes rolled sample is flat, indicating that the dissolution is uniform, conducive to promoting the self-peeling of discharge products. The results show that the samples with four passes of rolling have high electrochemical activity and anode efficiency. The average cell voltage and anodic efficiency of the four passes rolled anode for Mg-air battery within 5 h at 10 mA cm^{-2} were 1.065 V and 56.4%, respectively. Therefore, the electrochemical performance of the four passes rolled sample is the best, and the process is more suitable for preparing magnesium alloy anode plate.

Keywords: magnesium anode, multi-pass rolling, corrosion behavior, discharge performance, magnesium-air battery

Introduction

Magnesium alloys are widely used in aerospace, communication, and transportation because of their advantages of low cost and high specific strength. In addition, magnesium alloy has lower electrode potential (−2.37 V (*vs*. standard hydrogen electrode)), higher chemical activity, and theoretical capacitance (2.2 A h g^{-1}), which has attracted widespread attention in the field of chemical power supply.[1-3] However, magnesium alloy as anode material has some disadvantages, such as serious self-corrosion, self-discharge, and passivation in aqueous solution, which reduces its stability and anode efficiency.[4-6] In addition, during the reaction process, corrosion products adhere to the surface of the anode, which hinders the further reaction of the magnesium matrix and makes the potential shift positively, resulting in voltage lag.[7-9] Therefore, it is imperative to find magnesium alloy anode materials with high anode utilization.

At present, the most effective method to improve the performance of magnesium anode is alloying. Liu *et al.*[10] found that after adding Ca, Sm, and La to AZ91, the second phase was refined and dispersed, thus enhancing the voltage stability and discharge performance. The addition of Pb, La, and other elements was conducive to forming the formation of the β-Al_{11}-La_3 phase, which accelerates the matrix's active dissolution during depolarization, promoting the self-striping of oxidation products further accelerating the discharge activity of Mg-Al-Pb-La alloy.[11] In addition, heat treatment and plastic deformation can also change the microstructure of magnesium anode, thereby improving its discharge performance. Li *et al.*[12] carried out heat treatment on AZ63 magnesium alloy, which enhanced the adhesion of corrosion products on its surface, thus improving the corrosion resistance and electrochemical performance.

*e-mail: zhiquanhuang@tyust.edu.cn
Editor handled this article: Rodrigo A. A. Muñoz (Associate)

Yang *et al*.[13] rolled Mg-Al-Pb-La magnesium alloy, which resulted in reducing recrystallization degree and the second phase's fragmentation, thus enhancing the discharge activity. However, heavy metals in the alloy elements quickly pollute the environment in the operation process, the process flow is complex, and the cost is high. By contrast, plastic deformation entails a low price and is easy to implement; hence this method is the best choice for improving the electrochemical performance of magnesium alloys.

Plastic deformation includes processes such as extrusion and rolling. Among them, rolling can refine the grain size of magnesium alloy, reduce the texture strength, and change the grain structure and defects.[14,15] Magnesium alloys exhibit different microstructures (grain, substructure, etc.) under different rolling processes (temperature, total reduction, deformation between passes, etc.), resulting in different anode properties. There are few studies on the effect of pass deformation on the electrochemical performance of magnesium alloy anode. This paper studied the impact of different rolling passes on microstructure, corrosion behavior, and electrochemical performance of AZ31 magnesium alloy anodes for Mg-air batteries. This investigation is significant for wrought magnesium alloys as anodes for Mg-air batteries.

Experimental

Material preparation

Plates with dimensions of 100 mm × 100 mm × 10 mm were prepared from AZ31 magnesium alloy ingots, a double-roll mill for multiple rolls of passes. Before rolling, the plates were heated to 350 °C in a heating furnace and kept for 30 min. In this experiment, AZ31 magnesium alloy was rolled from 10 to 4 mm by four different rolling processes of two, three, four, and five passes, with a total deformation rate of 60%. The average pass reduction rates of two, three, four, and five passes were 36.5, 26, 20, and 16.5%, respectively. The specific rolling parameters are as follows: the rolling temperature is 350 °C, the rolling speed is 0.1 m s^{-1}, the samples are returned to the furnace for 15 min between each pass to ensure no deviation between the rolling temperature and the set temperature.

Chemicals

The chemicals used in this experiment mainly include solid sodium chloride, acetic acid, ethanol, picric acid, silver nitrate, and chromium oxide. The above chemicals were purchased from the Dazhong Chemical Reagent Market in Taiyuan, Shanxi Province, China.

Microscopic measurements

The metallographic samples were extracted from the rolled plates and polished step by step with 400, 600, 800, 1200, 1600 sandpaper. The samples were washed with absolute ethanol and then polished by the polishing machine. The polished samples were eroded with the corrosive mixture of 5 g picric acid, 100 mL ethanol, 5 mL acetic acid, and 10 mL distilled water and scanned with the spectrometer electron microscope (Zeiss group in Ober Kohen, Germany) to observe the grains, grain boundaries and intergranular precipitates of AZ31 magnesium alloy.

Electrochemical test

The electrochemical test samples were extracted from the middle of the rolled plates by wire cutting. The samples were exposed to 3.5% sodium chloride solution at room temperature. Electrochemical tests were carried out on the CHI760E electrochemical workstation (Shanghai Chenhua Instrument Co., Ltd. in Shanghai, China) with a traditional three-electrode system. The rolled plates were used as the working electrode, platinum plate as the auxiliary electrode and saturated calomel electrode (SCE) as the reference electrode. One end of the sample was welded with wires and sealed with epoxy resin, leaving only 1 cm^2 working area. The rolled plates were immersed in 3.5% NaCl solution for 5 min before the test to obtain a stable open-circuit potential. The potential scanning range of the dynamic potential polarization test was −2.5 V ca. −0.8 V, and the scanning rate was 10 mV s^{-1}. The experimental data were fitted by Cview software, and relevant parameters such as corrosion potential, corrosion current density, corrosion rate, and Tafel slope were obtained. The frequency range from 10^5 to 0.1 Hz was measured with the disturbance voltage amplitude of 5 mV. ZSimpWin software was used to analyze and fit the measured experimental data.

Mg-air battery test

The battery tests were performed using LAND Battery Test System (Wuhan LAND Electronic Co. Ltd. in Wuhan, China) with model CT2001A. For each magnesium air cell, the air electrode of $Ag/MnO_2/C$ catalyst (1 mg cm^{-2}) was used as the cathode, and the electrolyte was 3.5% NaCl aqueous solution, four magnesium alloy samples were used as anodes, and their performance was evaluated by constant current discharge at 2.5, 5, 10 and 20 mA cm^{-2}, the stationary discharge period of five hours was recorded. Before the test, the magnesium alloy anodes were sanded with 1800 sandpaper to remove surface oxides. The

200 g L^{-1} CrO_3 was used to clean the discharge products, and the anode efficiency and anode capacity density were calculated by the mass loss method. The scanning electron microscope (SEM) was used to observe the surface morphology of the anode after discharge.

Results and Discussion

Microstructure

Figure 1 shows the microstructure of AZ31 magnesium alloy after four different rolling passes. Figure 1a shows that the as-cast AZ31 magnesium alloy is composed of α-Mg matrix and coarse β-$Mg_{17}A_{12}$ phase distributed in the α-Mg matrix. With the increase of rolling passes, the grain size first decreases and then increases. Liu *et al.*[16] found that when the rolling temperature was 150, 200, 250, and 300 ºC, the critical pass deformation of fully dynamic recrystallization of the AZ31 magnesium alloy sheet was 52.7, 49.2, 34.3, and 32.9%, respectively, and the increase of rolling temperature reduced the critical pass deformation for fully dynamic recrystallization. The microstructure changed from coarse recrystallized microstructure to deformed microstructure, and the grains were significantly refined. The rolling temperature is 350 ºC, and the average pass deformation of the three rolling passes sample is 26%. Therefore, the grain refinement of the three rolling passes sample is the best (Figure 1c). Because the average deformation between passes (36.5%) is more significant than the critical deformation of fully dynamic recrystallization (26%), the average grain size no longer changes significantly with the increase of passes deformation, and the microstructure is slightly coarsened, compared with the three rolling passes sample, the grain size of the two rolling passes sample increases (Figure 1b).

The grains of four pass and five pass samples (Figures 1d and 1e) are refined, but the refinement effect is not as good as that of the three rolling passes sample. Compared with the three rolling passes deformation process, the reduction of each pass in the four rolling passes process is slight, and the deformation of the AZ31 plate is relatively uniform after multiple intermediate annealing. The cumulative strain is not as large as the previous process, and the grain refinement effect is poor. Complete dynamic recrystallization occurs in the four rolling passes sample, and the microstructure distribution of the plate after rolling is uniform, which approximately meets the standard normal distribution. Therefore, the grain

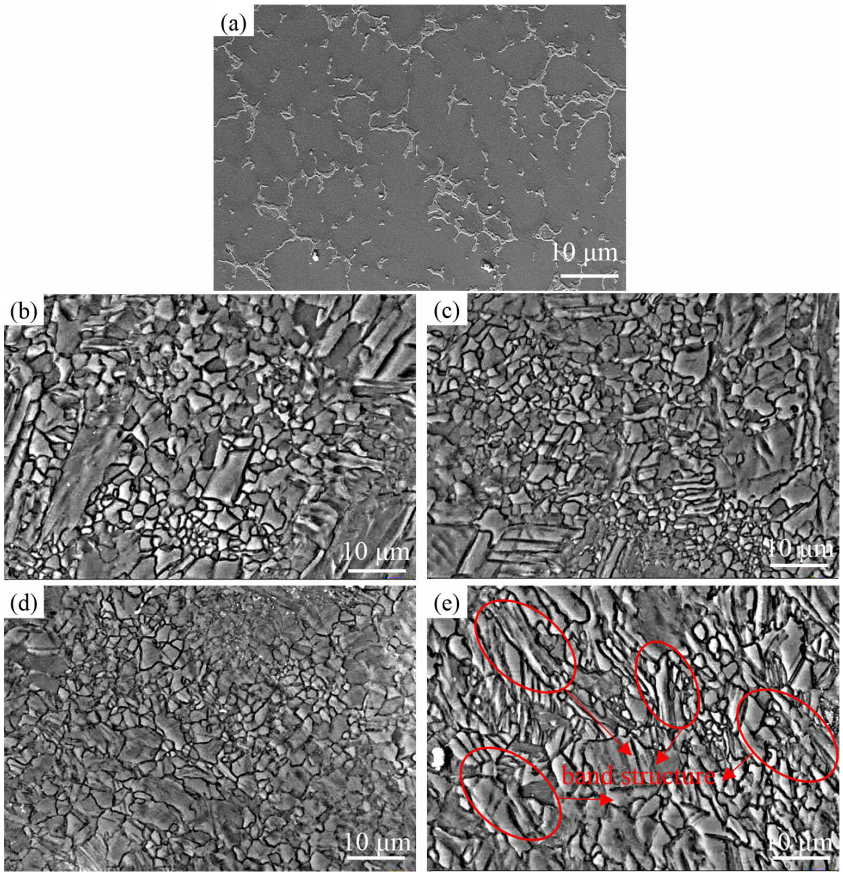

Figure 1. The microstructure of AZ31 magnesium alloy after four different rolling passes. (a) As-cast, (b) 2 passes, (c) 3 passes, (d) 4 passes and (e) 5 passes.

distribution of the four rolling passes sample is uniform. While the band structure of the five rolling passes sample is increased, the distribution is relatively scattered and has low distribution density. This is because the more times of heating and holding, the less noticeable the effect of rolling deformation on grain refinement. Huang *et al.*[9] studied the effect of twin density and deformation on the performance of magnesium air battery with AZ31 sheet as the anode. The energy density of the twin in the microstructure is high, the matrix begins to accelerate corrosion along with the twin, and the corrosion resistance of the electrode decreases to some extent.[17] In addition, there are some twins in the other three samples except for four passes rolled samples, which usually harm the electrochemical properties of the material.

Potentiodynamic polarization curve

Figure 2 shows the polarization curves of the investigated anodes in 3.5% NaCl solution, and electrochemical parameters are summarized in Table 1. It is well known that the anodic polarization curve is related to the dissolution of Mg, while the cathodic polarization curve is attributed to the hydrogen evolution reaction. Strong passivation can be observed in the anodic branches, which means that the anodic film (magnesium oxide and magnesium hydroxide corrosion product film) forms and acts as a physical shielding layer to prevent self-discharge of the anode. The corrosion potential (E_{corr}) arranges in order: two passes < four passes < five passes < three passes. The corrosion potential (E_{corr}) reflects the difficulty of corrosion initiation, and the negative corrosion potential means a high corrosion rate.[18] In addition, the corrosion current density (I_{corr}) arranges in an order: two passes > four passes > five passes > three passes. The corrosion current density (I_{corr}) is proportional to the corrosion rate.[19]

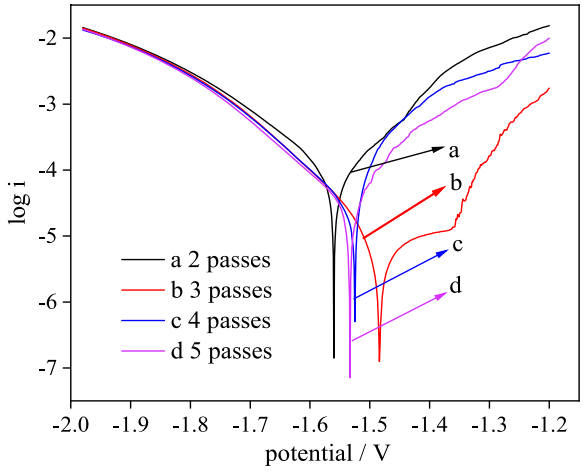

Figure 2. The potentiodynamic polarization curves of AZ31 magnesium alloy after four different rolling passes in 3.5% NaCl solution.

Table 1. Electrochemical data of all samples immersed in 3.5% NaCl solution calculated by Tafel extrapolation method

Sample code	E_{corr} / V	I_{corr} / (mA cm^{-2})	B_a / (mV dec^{-1})
2 passes	−1.56	9.54×10^{-5}	144.57
3 passes	−1.48	1.35×10^{-5}	124.76
4 passes	−1.54	2.96×10^{-5}	86.21
5 passes	−1.53	3.45×10^{-5}	132.46

E_{corr}: corrosion potential; I_{corr}: corrosion current density; B_a: Tafel anode slope.

Therefore, the corrosion rate of four different rolled passes from large to low is two passes > four passes > five passes > three passes.

Electrochemical impedance measurements

The electrochemical impedance spectra (EIS) curves of AZ31 magnesium alloy with four different rolling passes in 3.5% sodium chloride solution are shown in Figure 3. The Nyquist diagrams of the four samples are similar and include a high-frequency capacitive arc and a low-frequency inductive arc, the only difference is the diameter, which indicates that the corrosion mechanism is the same, but the corrosion rate is different. The capacitive reactance arc in the high-frequency region is related to the electric double-layer capacitance and the reaction transfer resistance. Due to the frequency dispersion effect, the capacitive reactance arc is not a perfect semicircle. Generally, the diameter of the capacitive loop is associated with the charge transfer resistance, which reflects the activity of the magnesium alloy electrode. The magnesium alloy electrode with small charge transfer resistance will show vigorous activity and be easier to activate and dissolve in the electrolyte under the corresponding test potential.[20] The low frequency induced reactance is caused by pitting corrosion or the chemical reaction of magnesium ions with water in the area without film coverage on the sample surface.[21] It can be seen from the coordinate value of the impedance spectrum in Figure 3a that with the increase of rolling passes, the diameter first increases and then decreases. The diameter of the sample with two passes is the smallest, which indicates that the sample has a strong corrosion rate. In addition, in the Bode diagram, the impedance modulus in the low-frequency region is related to the electrochemical activity, and the lower impedance modulus indicates higher electrochemical activity and more straightforward dissolution during discharge.[22] It can be seen from the Bode diagram in Figure 3b that with the increase of rolling passes, the impedance modulus of magnesium alloy in the low-frequency region (1 to 10 Hz) first increases and then decreases. Therefore, the two passes rolling sample has solid

electrochemical, and four passes follow. The electrochemical activity of the three rolling passes is the lowest. It is consistent with the polarization curve.

The electrical equivalent circuit diagram of magnesium alloy samples under four different rolling passes is shown in Figure 3c, where R_S is the solution resistance, R_T is the charge transfer resistance, and C is the interface capacitance of the double electric layer at the interface between the electrode and the solution. The constant phase angle element Q is often used to replace the capacitance.[23] The inductive reactance arc in the low-frequency region means desorption of the corrosion products, usually represented by inductance L and inductor resistance (R_L) in series.

The impedance data are fitted to the electrical equivalent circuit by ZSimpWin software, and the results are shown in Table 2. Due to the good electrical conductivity of sodium chloride solution, the R_S values of the four samples are close and relatively small. The charge transfer resistance (R_T) is proportional to its corrosion resistance.[24] The order of R_T values of four different rolled passes from large to small is three passes > five passes > four passes > two passes. In addition, the lower the Q value of magnesium alloy, the easier it is to form a thick and dense protective film on the surface of magnesium alloy.[25] The order of Q values of four different rolled passes from large to small is two passes > four passes > three passes > five passes. The loose oxide film is formed on its surface, conducive to the contact between the magnesium matrix and the electrolyte, thus enhancing the discharge performance. Therefore, the four passes rolled sample has good electrochemical activity. This conclusion is consistent with the previous test.

Corrosion appearance

Figure 4 shows the surface morphology of the four samples with different passes rolling after immersion in 3.5% NaCl solution for 24 h. The corrosion degree of the four samples from large to small is two passes >

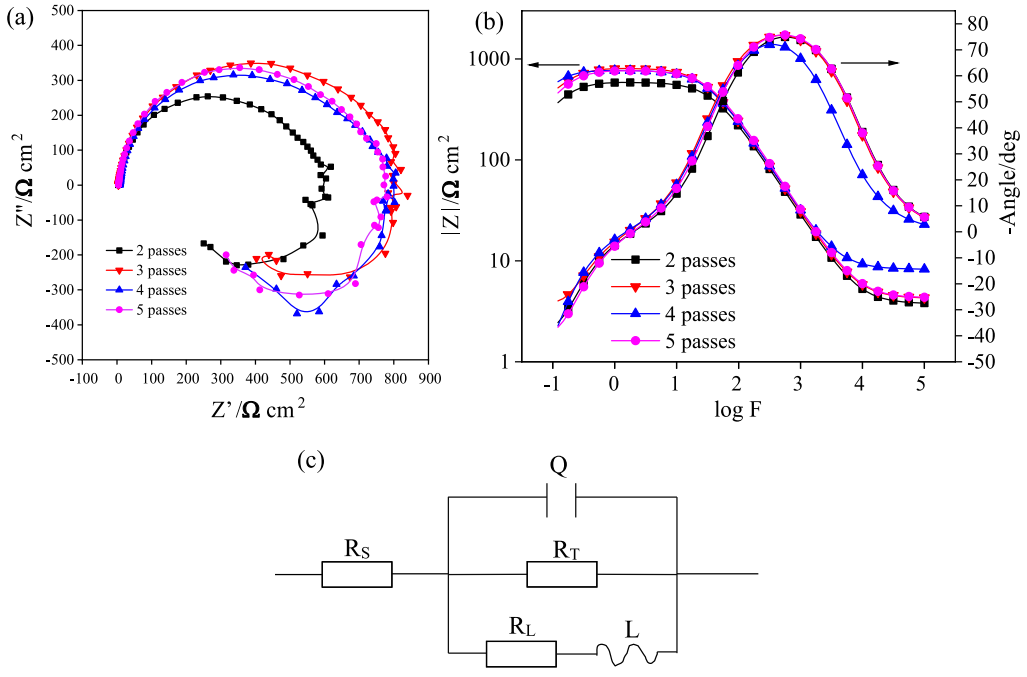

Figure 3. The electrochemical impedance spectra (EIS) curves of AZ31 magnesium alloy with four different rolling passes in 3.5% sodium chloride solution. (a) Nyquist diagram, (b) bode diagram and (c) equivalent circuit of fitting impedance spectrum.

Table 2. Electrochemical parameters obtained by electrochemical impedance spectroscopy fitting

Sample code	R_S / (Ω cm^2)	Q / (Ω^{-1} cm^{-2} s^n)	n	R_T / (Ω cm^2)	L / (Ω cm^2 s)	R_L / (Ω cm^2)
2 passes	3.76	1.03×10^{-5}	0.932	585.5	747.7	187.6
3 passes	4.24	9.81×10^{-6}	0.930	807.6	1128	484.8
4 passes	8.23	9.96×10^{-6}	0.929	764.9	1284	528.2
5 passes	4.29	8.89×10^{-6}	0.934	765.5	893.9	225.9

R_S: solution resistance; Q: interface capacitance of the double electric layer; n: equivalent to the dispersion factor; R_T: charge transfer resistance; L: inductance; R_L: inductance resistance.

four passes > five passes > three passes. As shown in Figure 4a, the surface of the two rolling passes sample is wholly corroded, and there are large cracks. The solution penetrates the magnesium alloy matrix through the cracks, aggravating the corrosion. The three rolled passes sample (Figure 4b) shows a more uniform and dense corrosion layer with fewer cracks and discontinuities. The formed corrosion layer prevents the matrix from further contacting the solution and plays a protective role. The corrosion products of the four rolled passes samples (Figure 4c) are loose and uniformly distributed in sheets. It can be seen from Figure 4d that the surface corrosion degree of five rolling passes sample is second only to three passes, with only minor cracks and more corrosion products.

The corrosion rate of magnesium alloy is usually related to the size and uniformity of the grains. Especially when 3.5% NaCl solution is used as the corrosive medium, the size of the grain affects the chemical activity and energy of the material.[26] Zheng *et al*.[27] studied the effect of grain size on the electrochemical performance of pure magnesium. Alloy stacking faults and defects usually affect the reaction process of the cathode, which may increase the volume fraction of the effective cathode, thus affecting the corrosion rate of magnesium alloy.[28] Large size microstructure and residual stresses adversely affect the corrosion behavior, while grain refinement positively affects corrosion behavior.[29] Four rolling passes is suitable for preparing magnesium anode because of its moderate grain size and uniform distribution, conducive to the stable discharge voltage. In addition, after multi-pass rolling, the internal alloy layer faults and defects are reduced, thus enhancing the corrosion rate. The corrosion products are porous layered structure and easy to separate from the surface of magnesium matrix, which reduce the polarization and increase the efficiency of anode.

Mg-air battery performance

Figure 5 shows the galvanostatic discharge curves for the four kinds of rolling pass samples discharged in 3.5% NaCl solution under different current densities. It can be seen from Figure 5 that the discharge voltages of the four samples shifted toward the negative direction in the initial stage of discharge. The reason for this phenomenon is that the electrochemical activity of magnesium is relatively strong, the discharge products quickly cover the surface of the sample, and Cl^- cannot go through the oxide film to reach the surface of the magnesium anode, which leads to a negative shift in the discharge potential.[30] In normal conditions, the discharge potentials became relatively stable with time, indicating that the accumulation and shedding of discharge products attain a dynamic balance.[31] However, as shown in Figures 5a and 5b, when the discharge current density is 2.5 and 5 mA cm^{-2}, the discharge curves of the four samples are always unstable. The discharge voltage decreases with time, indicating that the new reaction area of the samples is decreased, which is due to the

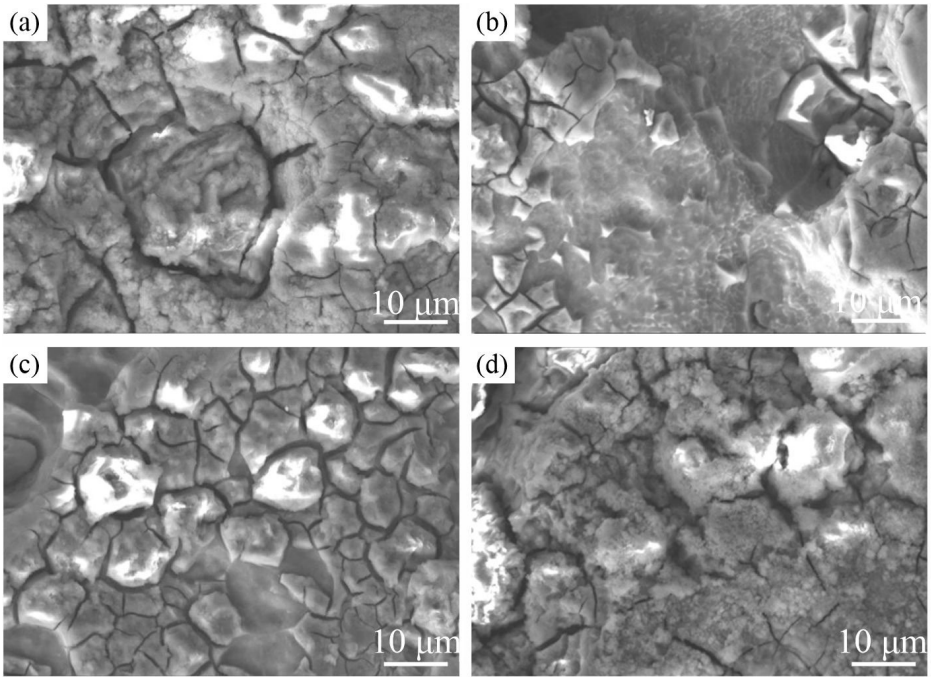

Figure 4. The surface morphology of the four samples with different passes rolling after immersion in 3.5% NaCl solution for 24 h. (a) 2 Passes, (b) 3 passes, (c) 4 passes and (d) 5 passes.

destruction of the balance between the accumulation and shedding of discharge products. The rate of generation of discharge products is greater than that of shedding. It is worth noting that all the samples studied have a stable discharge voltage platform at the discharge current density of 10 mA cm^{-2}. As shown in Figure 5d, when the discharge current density is 20 mA cm^{-2}, there is almost no difference in the discharge voltage of the anode studied, and the discharge curves are unstable. The research showed that AZ31 alloy was suitable for discharging power at low current density. When the discharge current density is greater than the limit of the material, the discharge stability will be broken. The magnesium alloy with four rolling passes has the highest discharge voltage. Since the experimental conditions are consistent, the higher and steadier potential of anode materials usually signifies the more vital discharge ability.

Table 3 shows the corresponding discharge parameters. Independent of the current density, with the increase of rolling passes, the anode efficiency of the studied anodes first increases and then decreases, and reaches the maximum in four passes. The anode efficiency of as-cast AZ31 is lower than the experimental results,[32] indicating that the anode efficiency of magnesium alloy can be improved by rolling, which is consistent with the previous research results. In addition, the results of this study show that the increase of rolling passes can improve the anode efficiency to a certain extent, but they are not proportional to each other. The discharge performance is related to the type of material, the number of twins, grain size, and grain uniformity.[33-35] As discussed in the "Microstructure" sub-section, compared with other rolling passes, the grains in the four passes sample are refined and uniformly distributed, and the dislocation slip is entirely carried out. Therefore, the four rolled passes sample has excellent discharge properties (discharge voltage of 1.065 V and anodic efficiency of 56.4%) at 10 mA cm^{-2}.

Surface morphologies after the discharge

The SEM photos of the anode surface morphology of four magnesium anodes after discharge with removal of the discharge products are displayed in Figure 6. There are several large pits on the surface of the discharged two passes rolled sample (as shown by the red arrows in Figure 6b), indicating that a large number of unreacted metal particles in the anode fall off ("chunk effect"). In addition, the anode self-corrosion during the discharge

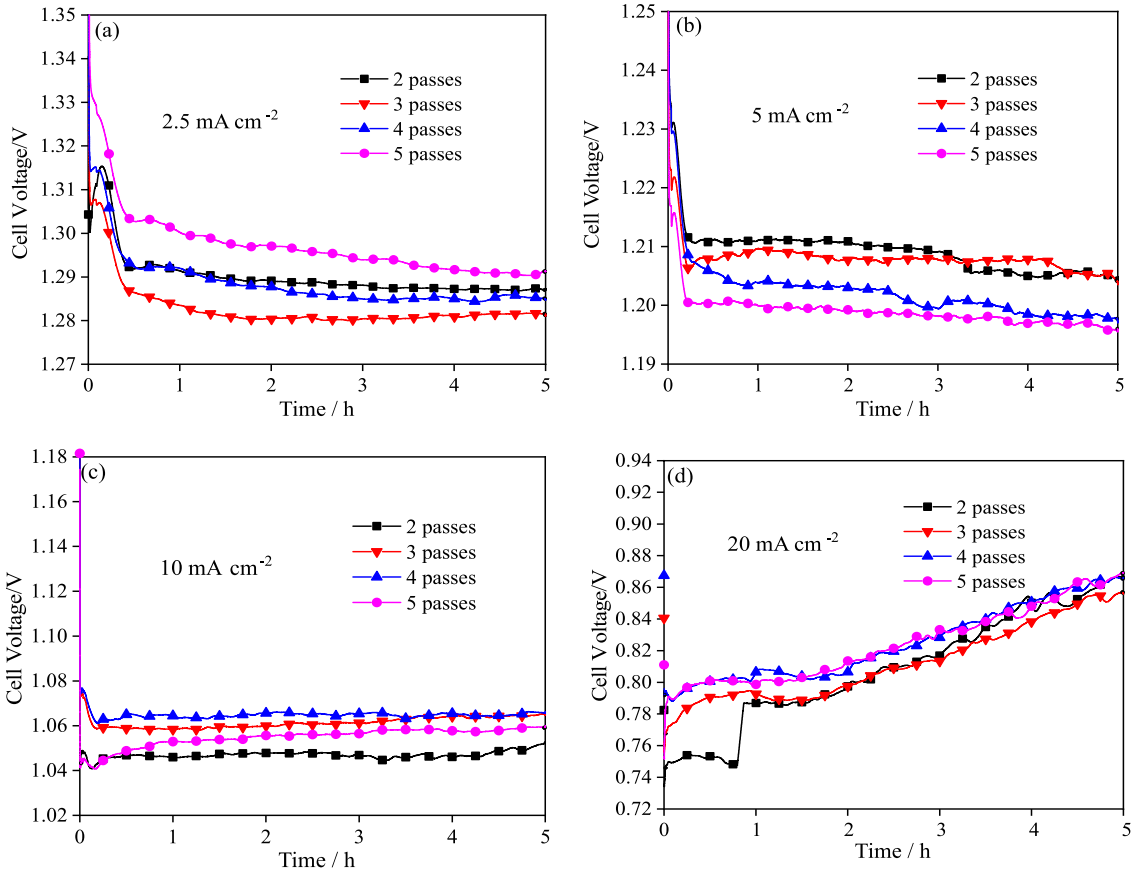

Figure 5. Discharge curve of AZ31 magnesium alloy in 3.5% NaCl under different rolling passes.

Table 3. Discharge parameters of Mg-air batteries with different anode under various current densities

Current density / (mA cm^{-2})	Alloy anode	Anode efficiency / %	Capacity density / (mA h g^{-1})	Energy density / (mW h g^{-1})	Reference
2.5	as-cast AZ31	33.998	759.109	649.663	36
	2 passes	48.831	1068.376	1376.841	this work
	3 passes	52.415	1146.789	1471.378	this work
	4 passes	52.901	1157.407	1493.269	this work
	5 passes	50.559	1106.195	1435.254	this work
5	as-cast AZ31	38.598	862.069	934.597	36
	2 passes	51.938	1136.364	1374.157	this work
	3 passes	53.471	1126.126	1360.376	this work
	4 passes	55.468	1213.592	1455.079	this work
	5 passes	52.011	1116.071	1341.948	this work
10	as-cast AZ31	44.185	986.842	1062.888	36
	2 passes	55.201	1207.729	1264.399	this work
	3 passes	54.282	1187.648	1264.608	this work
	4 passes	56.427	1243.568	1310.428	this work
	5 passes	55.401	1217.729	1273.913	this work
20	as-cast AZ31	51.762	1156.069	821.879	36
	2 passes	56.149	1228.501	993.729	this work
	3 passes	56.848	1243.781	1010.053	this work
	4 passes	57.709	1262.626	1040.549	this work
	5 passes	56.427	1234.568	1018.216	this work

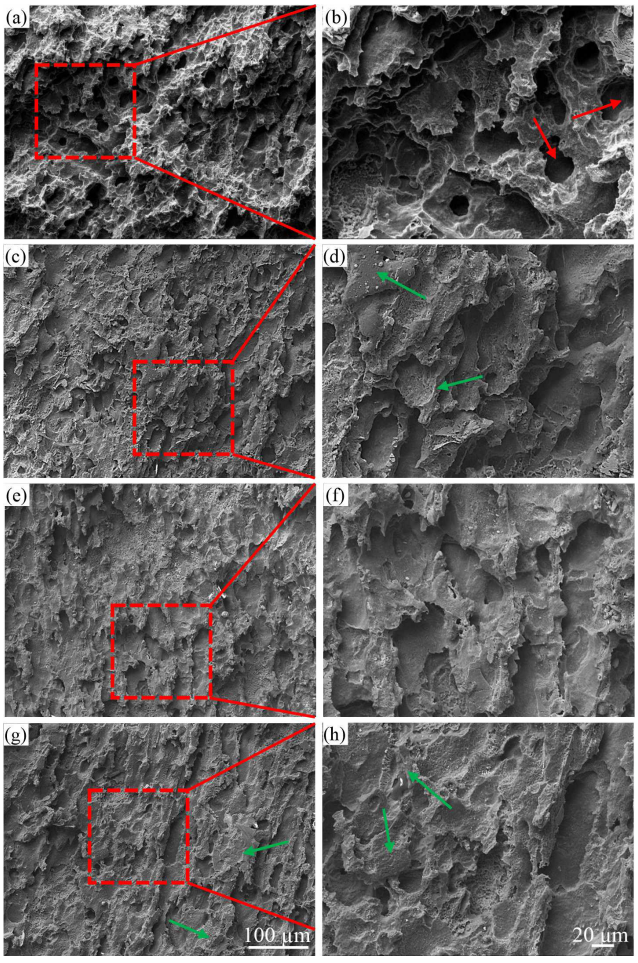

Figure 6. Surface morphologies of the anodes after discharge at 10 mA cm^{-2} for 5 h with removing of the discharge products. (a, b) 2 Passes, (c, d) 3 passes, (e, f) 4 passes and (g, h) 5 passes.

process also causes pits, which greatly wastes the anode and reduces the anode efficiency. As shown in Figure 6d, the discharged three passes rolled sample displayed a rough surface with a small amount of unreacted magnesium matrix (as indicated by the green arrows), which means that the anode has undergone a local reaction, and the surface morphology of the five passes rolled sample is similar to it (Figure 6h). On the contrary, as shown in Figure 6f, the discharged surfaces of the four passes rolled sample appears much flatter and has less local corrosion behavior, indicating the most uniform dissolution, which can effectively improve the anode efficiency of the magnesium alloy.

Conclusions

This work studied the effects of different rolling passes on the electrochemical and discharge properties of AZ31 magnesium alloy anode materials. The experimental results show that the grain size decreases first and then increases with rolling passes. The grain size of the four passes rolled sample is refined and evenly distributed, accompanied by a small number of twins. Compared with other passes, four passes rolled sample has the best discharge performance, with an anode efficiency of 56.4% and an energy density of 1243.568 mWh g^{-1} at the current density of 10 mA cm^{-2}. The excellent discharge performance is attributed to the uniform distribution of crystal grains that can make the Mg matrix uniformly dissolved in the electrolyte, which is conducive to the peeling of the discharge products. Meanwhile, a small number of twins positively affect the activity of magnesium alloys.

Acknowledgments

This research was funded by the National Natural Science Foundation of China (52075357), the National Key Research and Development Plan (2018YFA0707301), and Project supported by the open fund of State Key Laboratory of high-performance complex manufacturing, Central South University (Kfkt2019-03), The Graduate Education Innovation Project of Shanxi Province (2021Y672 and 2021Y687).

References

1. Li, C. Q.; Zeng, Z. R.; Sheng, L. Y.; Chen, X. B.; *Mater. Design.* **2017**, *121*, 430. [Crossref]
2. Peral, L. B.; Zafra, A.; Bagherifard, S.; Guagliano, M.; Fernández-Pariente, I.; *Surf. Coat. Tech.* **2020**, *401*, 126285. [Crossref]
3. Cheng, S. M.; Cheng, W. L.; Gu, X. J.; Yu, H.; Wang, Z. F.; Wang, H. X.; Wang, L. F.; *J. Alloys Compd.* **2020**, *823*, 153779. [Crossref]
4. Liu, H. L.; Tong, Z. P.; Zhou, W. F.; Yang, Y.; Jiao, J. F.; Ren, X. D.; *J. Alloys Compd.* **2020**, *846*, 155837. [Crossref]
5. Sun, L.; Ma, Y.; Wang, J. S.; An, L. Y.; Wang, S.; Wang, Z. Y.; *Surf. Coat. Technol.* **2020**, *390*, 125661. [Crossref]
6. Darband, G. B.; Alifkhazraei, M.; Hamghalam, P.; Valizade, N.; *J. Magnesium Alloys* **2017**, *5*, 74. [Crossref]
7. Chen, X. R.; Le, Q. C.; Atrens, A.; *J. Power Sources* **2020**, *451*, 227807. [Crossref]
8. Xiong, H. Q.; Yu, K.; Yin, X.; Dai, Y. L.; Yan, Y.; Zhu, H. L.; *J. Alloys Compd.* **2017**, *708*, 652. [Crossref]
9. Huang, G. S.; Zhao, Y. C.; Wang, Y. X.; Zhang, H.; Pan, F. S.; *Mater. Lett.* **2013**, *113*, 46. [Crossref]
10. Liu, X.; Xue, J. L.; Zhang, P. J.; Wang, Z. J.; *J. Power Sources* **2019**, *414*, 174. [Crossref]
11. Feng, Y.; Lei, G.; He, Y. Q.; Wang, R. C.; Wang, X. F.; *Trans. Nonferrous Met. Soc. China* **2018**, *28*, 2274. [Crossref]
12. Li, J. R.; Jiang, Q. T.; Sun, H. Y.; Li, Y. T.; *Corros. Sci.* **2016**, *111*, 288. [Crossref]
13. Yang, M.; Shi, Y. C.; Chen, W. Z.; Wang, R. C.; Feng, Y.; *Trans. Nonferrous Met. Soc. China* **2017**, *8*, 1603. [Crossref]
14. Liu, D.; Liu, Z. Y.; Wang, E. D.; *Mater. Sci. Eng., A* **2014**, *612*, 208. [Crossref]
15. Fan, C. H.; Zheng, D. S.; Chen, X. H.; Yang, J. J.; Liu, Y.; Li, H. Z.; *Trans. Nonferrous Met. Soc. China* **2019**, *29*, 263. [Crossref]
16. Liu, D.; Liu, Z. Y.; Wang, E. D.; *Trans. Nonferrous Met. Soc. China* **2015**, *25*, 3585. [Crossref]
17. Aung, N. N.; Zhou, W.; *Corros. Sci.* **2010**, *52*, 589. [Crossref]
18. Liu, H.; Yan, Y.; Wu, X. H.; Fang, H. J.; Chu, X.; Huang, J. F.; Zhang, J. X.; Song, J. M.; Yu, K.; *J. Alloys Compd.* **2020**, *859*, 157755. [Crossref]
19. Chen, X. R.; Jia, Y. H.; Le, Q. C.; Wang, H. N.; Zhou, X.; Yu, F. X.; Atrens, A.; *J. Magnesium Alloys* **2020**, *9*, 2113. [Crossref]
20. de Oliveira, L. A.; da Silva, R. M.; Rodas, A. C.; Souto, R. M.; Antunes, R. A.; *J. Mater. Res. Technol.* **2020**, *9*, 14754. [Crossref]
21. Ma, J. L.; Zhang, Y.; Ma, M. S.; Qin, C. H.; Ren, F. Z.; Wang, G. X.; *Corros. Sci.* **2020**, *170*, 108695. [Crossref]
22. Huang, H. L.; Yang, W. L.; *Arabian J. Chem.* **2020**, *13*, 6044. [Crossref]
23. Hlongwa, N. W.; Ikpo, C.; Ross, N.; Nzaba, M.; Ndipingwi, M.; *J. Nano Res.* **2016**, *44*, 90. [Crossref]
24. Ma, H. J.; Gu, Y. H.; Liu, S. J.; Che, J. T.; Yang, D. W.; *Surf. Coat. Technol.* **2017**, *331*, 179. [Crossref]
25. Pokharel, D. B.; Wu, L. P.; Dong, J. H.; Yadav, A. P.; Subedi, D. B.; Dhakal, M.; Zha, L.; Mu, X.; Umoh, A. J.; Ke, W.; *J. Mater. Sci. Technol.* **2021**, *81*, 97. [Crossref]
26. Wang, N. G.; Mu, Y. C.; Xiong, W. H.; Zhang, J. C.; Li, Q.; Shi, Z. C.; *Corros. Sci.* **2018**, *144*, 107. [Crossref]

27. Zheng, T. X.; Hu, Y. B.; Yang, S.W.; *J. Magnesium Alloys* **2017**, *5*, 404. [Crossref]
28. Wang, B. J.; Xu, K.; Xu, D. K.; Cai, X.; Qiao, Y. X.; Sheng, L. Y.; *J. Mater. Sci. Technol.* **2020**, *53*, 102. [Crossref]
29. Liu, F. J.; Ji, Y.; Sun, Z. Y.; Liu, J. B.; Bai, Y. X.; Shen, Z. K.; *J. Alloys Compd.* **2020**, *829*, 154452. [Crossref]
30. Tong, F. L.; Chen, X. Z.; Wang, Q.; Wei, S. H.; Gao, W.; *J. Alloys Compd.* **2021**, *857*, 157579. [Crossref]
31. Wu, J. L.; Wang, R. C.; Feng, Y.; Peng, C. Q.; *J. Alloys Compd.* **2018**, *765*, 736. [Crossref]
32. Li, Q.; Xiong, W.; Yu, M. H.; Li, J.; Liu, L.; Zhu, G.; Wang, L. Y.; Wang, J.; Yu, S. R.; Liu, E. Y.; *J. Alloys Compd.* **2022**, *891*, 161914. [Crossref]
33. Wang, N. G.; Li, W. P.; Huang, Y. X.; Wu, G.; Hu, M. C.; Li, G. Z.; Shi, Z. C.; *J. Power Sources* **2019**, *436*, 226855. [Crossref]
34. Cheng, P.; Chen, Y. G.; Ding, W. C.; *Mater. Sci. Forum* **2017**, *904*, 80. [Crossref]
35. Prince, L.; Rousseau, M. A.; Noirfalise, X.; Dangreau, L.; Coelho, L. B.; Olivier, M. G.; *Corros. Sci.* **2021**, *179*, 109131. [Crossref]
36. Deng, M.; Wang, R. C.; Feng, Y.; Wang, N. G.; Wang, L. Q.; *Trans. Nonferrous Met. Soc. China* **2016**, *26*, 2144. [Crossref]

Submitted: November 16, 2021
Published online: April 14, 2022